Annals of Nuclear Energy 59 (2013) 243–254

Contents lists available at SciVerse ScienceDirect

Annals of Nuclear Energy

journal homepage: www.elsevier.com/locate/anucene

A new experimental approach for subcritical reactivity determination of multiplying systems

Adimir Dos Santos *, Seung Min Lee, Ricardo Diniz, Rogério Jerez

Instituto de Pesquisas Energéticas e Nucleares, Av. Lineu Prestes 2242, CEP 05508-000 São Paulo, SP, Brazil

ARTICLE INFO

Article history:
Received 17 December 2012
Received in revised form 10 April 2013
Accepted 16 April 2013
Available online 15 May 2013

Keywords:
Reactor kinetics
Subcritical systems
Kinetic parameters
Reactivity
APSD

ABSTRACT

This work presents a new experimental approach to determine the reactivity levels of subcritical systems. The method employs the subcritical kinetic model developed by Gandini and Salvatores and it is based only on measured quantities such as counting rates of the detectors employed in the experiments and the parameters arising from the least squares fitting of the APSD (Auto Power Spectral Density). Detector efficiencies, quantity required in other procedures such as Neutron Source Multiplication (NSM) method, are not needed in the proposed method. The only hypothesis made in the method is the independence of the effective delayed neutron fraction and the prompt neutron generation time to the subcriticality level of the system. The proposed method was applied to measure the reactivity of several subcritical configurations of the IPEN/MB-01 reactor. Measurements of APSD were performed in several degrees of subcriticality (up to around −7000 pcm). The APSD data were least squares fitted to get the prompt decay mode (α) and other quantities. Beside the startup source of the facility, an external neutron source of Am–Be was installed near the core in order to improve neutron counting statistics. The final experimental results are of very good quality. The proposed experimental method shows clearly that the classical point kinetic theory cannot describe the measured reactivity. Instead, the reactivity inferred from this model follows closely the subcriticality index (ζ) for the source arrangements in the experiment. The agreement of the MCNP5 and GPT-TORT results, both with ENDF/B-VII.0 as the basic nuclear data library, when compared to the corresponding experimental ones was very good.

1. Introduction

In recent years there has been a great deal of interest in subcritical systems (Gandini and Salvatores, 2002; Salvatores et al., 1996). This interest was, in part, due to the development of hybrid concepts called ADS (Accelerator Driven System) (Rubbia et al., 2004) and also due to enormous interest in quantifying experimentally the reactivity when a reactor is in a subcritical state. The reactor physics tests of a PWR in which the reactor starts up and approaches criticality is one of the situations where the knowledge of the subcritical reactivity is of great importance. Before and during the tests, there are two important issues related to reactivity measurements. The first one is related to the subcritical measurements during the criticality approach. The monitoring and the prediction of the subcritical multiplication conditions are essential to assure that the operation of the control rod withdrawn or the boron dilution processes is carried out with safety in order to get criticality of the reactor core. Currently, there are several methods able to estimate when criticality will occur. One of these methods, called Neutron Source Multiplication (NSM) method (Shi et al., 2005), is performed by plotting the inversion ratio of the neutron counting rate, which is obtained from the source range detector as a function of the change in the condition being used to bring the reactor critical, e.g., boron dilution or control rod bank withdrawn. This method assumes that the neutron flux distribution is in the fundamental mode and its shape remains unchanged during the criticality approach. However, in a real situation, the neutron flux distribution is composed by the fundamental and higher harmonic modes. Furthermore, the neutron flux shape changes significantly with the subcritical level (Shimazu and Naing, 2005; Hoogenboom and Van der Sluijs, 1988). The second important issue in the reactor physics test is the control bank worth measurements which are conventionally carried out by the boron dilution method.

Another important application is the criticality safety analyses and the subsequent establishment of the uncertainties margins and possible bias in the effective multiplication factor. For this application the most common procedure is to analyze the appropriate ICSBEP (Briggs, 2012) benchmarks; i.e., the

* Corresponding author. Address: Instituto de Pesquisas Energéticas e Nucleares, IPEN/CNEN-SP, Centro de Engenharia Nuclear (CEN), Av. Prof. Lineu Prestes 2242, Cidade Universitária, 05508-000 São Paulo, SP, Brazil. Tel.: +55 11 3133 9479; fax: +55 11 3133 9423.

E-mail addresses: asantos@ipen.br (A. Dos Santos), smlee@ipen.br (S.M. Lee), rdiniz@ipen.br (R. Diniz), rjerez@ipen.br (R. Jerez).

0306-4549/$ - see front matter © 2013 Elsevier Ltd. All rights reserved.
http://dx.doi.org/10.1016/j.anucene.2013.04.015

benchmarks that resemble or that are very similar to the application under consideration. However, the analyses of the ICSBEP benchmarks rely mostly in critical systems and the uncertainty and possible bias in the subcritical situations is taken the same as the critical systems which might incur in some errors.

The subcritical reactivity is closely related to the kinetic model applicable to the system. Several models (Gandini, 2004; Dulla et al., 2006) were proposed to characterize the kinetics of subcritical reactors especially in regard to the reactivity of the system. Theoretical models suggest the unfolding of the system reactivity into two components: first, the reactivity of a system as normally obtained through the generalized perturbation theory (Gandini, 2001) and second, the reactivity due to the source present in the system. This last component is extremely complex to obtain experimentally since the detector's efficiency is altered when the subcriticality level of the system changes.

Besides the difficulties already mentioned, a major complicating factor in the verification and validation of the proposed models that deal with subcritical systems is the lack of experimental data providing appropriate physical quantities that could be described and treated by these models. In this aspect the IPEN/MB-01 reactor can be of extreme importance because it is an installation with very well established geometric features and material content. The IPEN/MB-01 reactor has been considered an international benchmark in various experiments of critical configurations (Dos Santos et al., 2004; Dos Santos et al., 2008) as well as in several reactor physics experiments (Dos Santos et al., 2009). Thus, the IPEN/MB-01 reactor can be considered extremely important for developing experimental methods and establishing experimental parameters for the validation of kinetic models for subcritical systems.

The purpose of this work is to present a new method to measure subcritical reactivity of a multiplying system based on the subcritical kinetic model of Gandini and Salvatores (Gandini and Salvatores, 2002; Gandini, 2004). The kinetic equations of this model are employed to write down the Auto Power Spectral Density (APSD) from where the subcritical parameters are obtained. The proposed method relies only on measured quantities. Quantities difficult to be determined such as detector efficiency are not required in this approach.

2. Theory

The kinetic equations of the Gandini and Salvatores (Gandini and Salvatores, 2002) method are given by:

$$l_{eff}\frac{dP_N(t)}{dt} = (\rho_{gen} - \alpha_{pd}\beta_{eff})P_N(t) + \sum_{i=1}\lambda_j\xi_j(t) + \zeta(1 - P_N(t)) + \rho_{source} \tag{1}$$

and

$$\frac{d\xi_j(t)}{dt} = \beta_{eff\,j}P_N(t) - \lambda_j\xi_j(t) \tag{2}$$

where l_{eff} is the prompt neutron generation time, $P_N(t)$ the relative power of the reactor, ρ_{gen} the generalized reactivity; i.e. the reactivity arising from the generalized perturbation theory (GPT) (see Section 6 for the mathematical definition), α_{pd} the relation between prompt and delayed neutron spectra, β_{eff} the effective fraction of delayed neutrons, $\beta_{eff,j}$ the effective fraction of jth family of delayed neutrons, λ_j the precursor decay constant for the jth family of delayed neutrons, ξ_j the concentration of the precursor of the jth family of delayed neutrons, ζ the subcriticality index, and ρ_{source} is the reactivity due to variation of the source.

The resemblance of Eqs. (1) and (2) to the usual point kinetic equations is only apparent, and they should be used with care since the relative power makes a big difference between the models.

Through Eqs. (1) and (2), and by using standard procedures (Hetrick, 1971; Bell and Glasstone, 1979), a zero-power reactor transfer function can be readily written as:

$$G(\omega) = \frac{1}{\alpha_{pd}\sum_{j=1}^{6}\frac{i\omega\beta_{eff\,j}}{(i\omega-\lambda_j)} - i\omega l_{eff} - \rho_{gen} + \zeta} \tag{3}$$

where ω is the angular frequency, and it was assumed that there are six groups of delayed neutrons.

Over a frequency region where $\omega >> \lambda_i$, Eq. (3) can be simplified to

$$G(\omega) = \frac{1}{\alpha_{pd}\sum_{j=1}^{6}\beta_{eff\,j} - i\omega l_{eff} - \rho_{gen} + \zeta} = \frac{1}{\alpha_{pd}\beta_{eff} - i\omega l_{eff} - \rho_{gen} + \zeta} \tag{4}$$

Now, considering a standard electronic chain for a pulse-mode detector, the APSD of the neutron noise is given by:

$$\Phi(\omega) = \frac{A}{\omega^2 + B^2} + C \tag{5}$$

where A and C are constants, being C the uncorrelated or detection noise, and

$$B = \frac{\rho_{gen} - \alpha_{pd}\beta_{eff} - \zeta}{l_{eff}} \tag{6}$$

is the analog of the prompt decay constant α for the usual point kinetic model.

The parameters A, B and C can be obtained by fitting the experimental APSD through a least squares procedure.

Furthermore, in a steady state condition Eqs. (1) and (2) yield,

$$\rho_{gen}P_N + \zeta(1 - P_N) + \rho_{source} = 0 \tag{7}$$

Through Eqs. (6) and (7), assuming $\rho_{source} = 0$, the parameters of interest, ζ and ρ_{gen}, are readily obtained as:

$$\zeta = -(Bl_{eff} + \alpha_{pd}\beta_{eff})P_N \tag{8}$$

$$\rho_{gen} = (Bl_{eff} + \alpha_{pd}\beta_{eff})(1 - P_N) \tag{9}$$

In Eqs. (8) and (9) the B parameter is obtained by a least squares approach, while l_{eff} and β_{eff} are already known from previous experiments (Dos Santos et al., 2009). l_{eff} and β_{eff} are assumed to be independent of the subcriticality level. In order to employ Eqs. (8) and (9), the relative power P_N of two consecutive states should be obtained. By analogy with the point kinetic model, the power for a certain state is given by (Cohn, 1960; Suzuki,1966):

$$P = \frac{2R^2(\gamma D)l_{eff}^{-2}}{(B)^2(\Phi^p - C)} \tag{10}$$

where R is the current changed to voltage if the detector is operating in current mode or counts if it is operating in pulse counting mode, γ the energy released per fission in Joule, D the Diven factor, B the prompt neutron decay constant α or its analog, depending on the kinetic model employed, Φ^p the mean value of the APSD on the first plateau level in V^2/Hz for current mode detector, or Counts^2/Hz for pulse mode detector, and C is the mean value of the uncorrelated noise.

Now, considering two states a and b, of which b is more subcritical than a, and assuming that l_{eff} is independent of the subcriticality levels, the relative power between these two states can be written as:

$$P_N = \frac{P_b}{P_a} = \frac{R_b^2B_a^2(\Phi_a^p - C_a)}{R_a^2B_b^2(\Phi_b^p - C_b)} \tag{11}$$

Thus, through Eqs. (8), (9), and (11) the parameters ζ and ρ_{gen} can be obtained in a purely experimental way. In Eqs. (8) and (9), α_{pd} is considered as unity for the purposes of this work.

3. APSD measurement method

A diagram of the electronic equipment and the data acquisition and processing system is illustrated in Fig. 1. According to this figure, neutron pulses from the detectors are formatted and amplified by preamplifiers and amplifiers, and subsequently discriminated from the γ-radiation through the Lower Level Discriminator of the single channel module (Single-Channel Analyzer – SCA). Negative logical pulses are generated in the output of the single channel (standard NIM fast negative) with 25 ns width and -5 V of amplitude on 50 Ω impedance. A multichannel scaler (MCS) board registers the logical pulses in a number of small time intervals – called dwell time. This procedure is totally analogous to the Kitamura's work (Kitamura et al., 1999). The minimum value for the dwell time of MCS is 100 ns and the number of channels can vary from 4 to 65,536. The dwell time provides the maximum frequency to be analyzed, and the number of channels gives the corresponding frequency resolution. In this work the dwell time was set at 2×10^{-4} s, which results in a maximum frequency of 2.5 kHz (single-sided spectrum), and the number of channels, in the time domain, was set to be 8192, which results in a resolution of nearly 0.61 Hz in the frequency domain. The record length – the time required to complete one acquisition – is $(2 \times 10^{-4})\,(8192) \cong 1.64$ s. Each experimental point of the APSD has an error bar given by $N^{-1/2}(\%)$, where N is the number of averages (Bendat and Piersol, 2000). In general, the number of averages ranged from 800 to 1000.

Fig. 2 shows the scheme of the time data acquisition by the MCS board for processing and obtaining the spectral densities.

Fig. 3 shows two typical APSDs obtained in a state close to critical and in a subcritical level of nearly -2600 pcm. The number of averages was around 1000 in both cases, and a more sensitive detector was employed in the subcritical case.

As can be seen from Fig. 3 the APSD's show the expected behavior for the reactivity. The α value, given as $(\rho - \beta)/l_{eff}$ in the classical point kinetic model, shifts to the right as the negative reactivity increases, and the ratio of correlated – first plateau – to uncorrelated – second plateau – noise decreases. It is also clear that the dispersion of data is higher in the subcritical case. The high dispersion of data in some subcritical states can be reduced by employing additional neutron sources, as described in the next section.

It can be concluded that, despite the higher fluctuations in some subcritical states, the data are of good quality, and they represent the physical aspects of the problem.

4. Experimental configuration and procedure

The experimental configuration is shown in Fig. 4 and it is one of the critical configurations of LEU.COMP.THERM.082 (Dos Santos, 2006). This figure also illustrates the configuration of the core of IPEN/MB-01 reactor used for this experiment. Symbols BC and BS refer respectively to the control and safety rods. There are two banks diagonally placed for each type. The standard core of the reactor consists of an array of 28×26 positions, out of that 680 are filled with fuel rods. For this experiment the outer row of fuel rods was removed in each face, i.e., 104 fuel rods. Thus almost all of reactivity excess was removed from the core (measured K_{eff} is equal to 1.00010, with control and safety banks completely withdrawn). The reactor core remained immersed in a demineralized light water tank during the whole operation. The reactivity was controlled by two control banks of Ag–In–Cd alloy. The safety banks of B_4C (BS in Fig. 4) are kept at a removal position of 135% (the absorber is at 35% of the active core length above the active core). Therefore, when the safety banks are in the totally withdrawn position, they have very little impact on the reactivity of the system. A detailed description of the IPEN/MB-01 reactor can be found in (Dos Santos, 2008). This new core configuration, of 26×24 fuel rods, was used for two reasons: firstly, to allow the

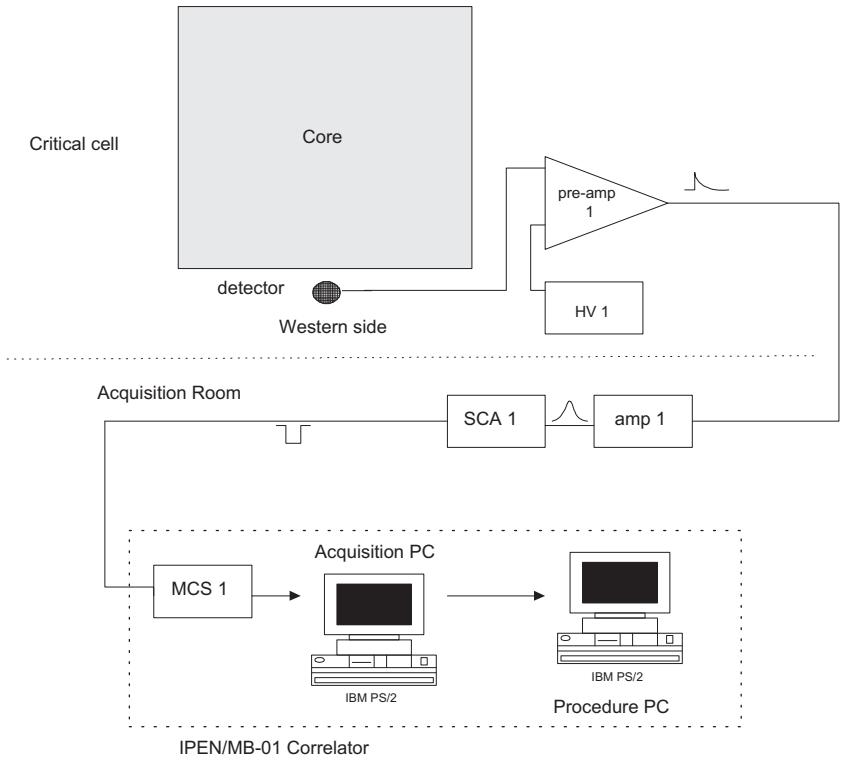

Fig. 1. Diagram of electronics and acquisition and data processing system of the IPEN/MB-01, used in noise analysis measurements.

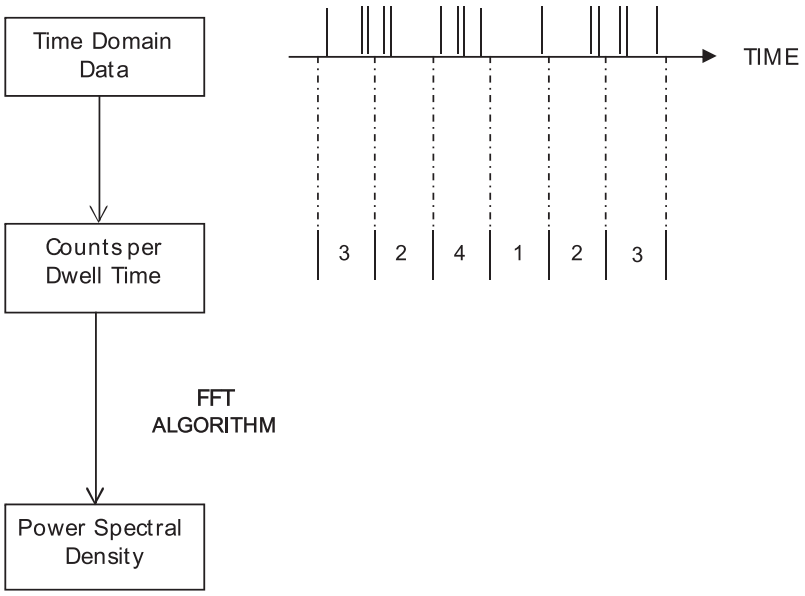

Fig. 2. Data processing scheme for obtaining the spectral densities.

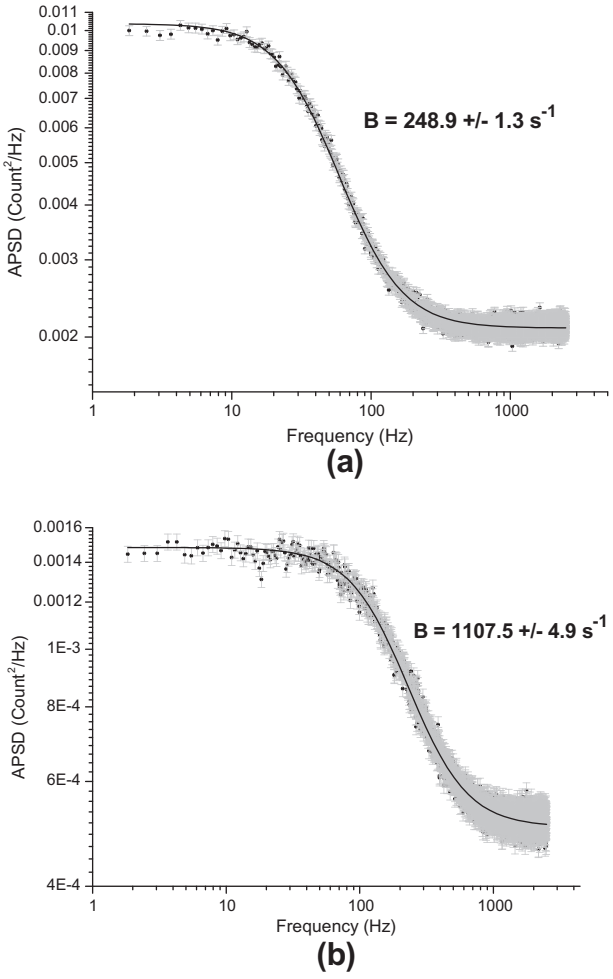

Fig. 3. Experimental APSD obtained in a near critical state (a) and in a subcritical (−2600 pcm) state (b). The black solid line is the least squares fitting through Eq. (5).

control banks to be initially at the outermost withdrawn position possible, and secondly, to get a subcriticality level as low as possible when the control rods are totally inserted.

The result shown in this paper considered the utilization of three pulse mode detectors: one of BF_3, near the criticality (from 0 to ∼−1700 pcm); another of ^{3}He, in the middle region (from −1900 to ∼−3200 pcm); the other of ^{3}He more sensitive, in the most subcritical region (from −3900 to ∼−7500 pcm). In order to reach this reactivity range (from 0 to −7500 pcm), the two control banks, BC1 and BC2 (always kept aligned), were inserted simultaneously in steps of 5% or 2.5% (the unit% represents the percentage of withdrawn length in relation to the total active length of the rods), depending on the differential worth of the bank at a given position. As shown in Fig. 4, the detectors were positioned, one at time, in the *y*–*z* plane and about 12 cm away from the outmost fuel rods. Also, their axial positions were always kept aligned to the *z*-direction.

In order to improve the statistics of the detectors counts, and so the resolution of the APSDs, additional external neutron sources of Am–Be of 100 mCi or 1 Ci were placed in the middle of the east face of the core, very close to the outermost fuel rod row as shown in Fig. 4. In all cases the startup source of 1 Ci Am–Be was inserted.

Depending on the control bank positions (in the sense of negative reactivity inserted), the detector sensitivity and the employment of extra neutron sources, the measurements were divided in four parts as shown in Table 1.

The measurements start with the two control banks at the position of 93% withdrawn. This position was chosen because of the compromise to have the control bank position as close as possible to the critical state, and the condition of no detector saturation. Any other position closer to that of the critical state would saturate the detector. Then, the control banks were simultaneously inserted in carefully chosen steps so that the counting rates in two consecutive states were significantly different, and also that the conditions for the validity of 1st order Perturbation Theory, which is the basis for the development of the subcritical kinetic model of Gandini and Salvatores, were not violated. In each of these subcritical states the APSD and counting rate were measured.

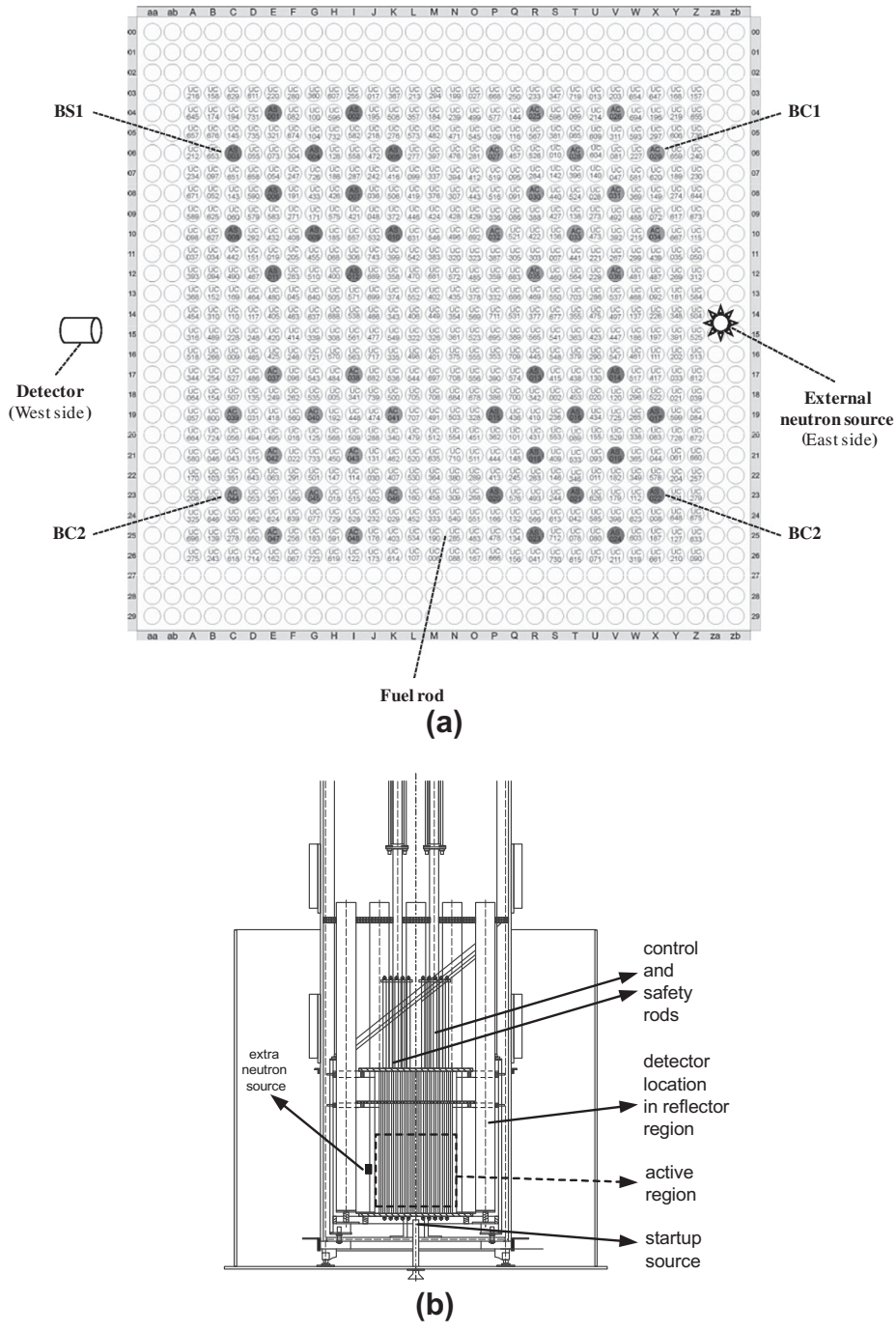

Fig. 4. Upper view (a) and side view (b) of the core of the IPEN/MB-01 reactor, showing detector and neutron source locations.

Table 1
Detectors and additional neutron sources employed in the experiments.

Bank positions (% withdrawn)	Detector employed	Extra neutron source
93–75.5	BF3 low sensitivity	100 mCi
70.5–65.5	BF3 low sensitivity	1 Ci
63–50.5	He3 medium sensitivity	2 Ci[a]
45.5–0	He3 high sensitivity	Ci

[a] Two sources of 1 Ci.

The temperature in the fuel region was monitored by means of a set of thermocouples, strategically located in the reactor core. The thermocouples are made of an alloy of Cu–Ni (55% Cu and 45% Ni) and their diameter is 1.6 mm. As in LEU.COMP.THERM.077 (Dos Santos et al., 2004), 12 thermocouples were used in the experiment. The thermocouples were calibrated by a standard procedure and the claimed accuracy for the absolute measurements is ±0.02 °C. The average temperature in the whole set of experiments was 19.6 ± 0.2 °C (1σ).

The uncertainty in the control bank positioning is mostly linked to the setting of its reference level as well as to the linearity of the acquisition system. The linearity of the control bank system is verified routinely and it has been proven to be adequate for the purposes of the experiment. The uncertainty in the control bank positioning was then mostly due to the accuracy of the mechanical

pattern to set the reference level. This uncertainty is equal to 0.1 mm; which represents less than 1.0 pcm and can be neglected in the whole uncertainty analysis of the experiment.

5. The experimental results

The parameters B and C in Eq. (11) were obtained by means of the least squares method. Φ^p, the upper plateau in Fig. 3, was obtained as the average of the measured values in that region of frequency. Therefore, P_N, the relative or normalized power, and, consequently, ρ_{gen} for each subcritical state relatively to the previous state and ζ, could be determined in a straightforward fashion. The reactivity of each state relative to the initial state was considered as the sum of partial ρ_{gen}, and it will be represented in this paper by $\Sigma\rho_{gen}$.

The values for β_{eff} and l_{eff} used in the experimental approach were extracted from the IRPhE Handbook (Dos Santos et al., 2009) and they are international benchmarks performed in the IPEN/MB-01 reactor for the determination of the effective delayed neutron parameters. The values used in the experiment were 0.00750(±0.00005) and 32.02(±1.06) μs, respectively, for β_{eff} and l_{eff}.

The uncertainties on ρ_{gen} and ζ were calculated through the standard error propagation of Eqs. (9) and (8), respectively as:

$$\sigma^2_{\rho_{gen}} = \left[(B_b l_{eff} + \beta_{eff})P_N\right]^2 \times \left[2^2\left(\frac{\sigma^2_{R_b}}{R_b^2} + \frac{\sigma^2_{R_a}}{R_a^2} + \frac{\sigma^2_{B_a}}{B_a^2}\right) + \frac{\sigma^2_{C_b} + \sigma^2_{\Phi_b}}{(\Phi_b - C_b)^2} + \frac{\sigma^2_{C_a} + \sigma^2_{\Phi_a}}{(\Phi_a - C_a)^2}\right] + \sigma^2_{B_b}\left[l_{eff} + P_N l_{eff} + \frac{2\beta_{eff}P_N}{B_b}\right]^2 + (1 - P_N)^2(B_b^2\sigma^2_{l_{eff}} + \sigma^2_{\beta_{eff}}) \quad (12)$$

$$\sigma^2_{\zeta} = \left[(B_b l_{eff} + \beta_{eff})P_N\right]^2 \times \left[2^2\left(\frac{\sigma^2_{R_b}}{R_b^2} + \frac{\sigma^2_{R_a}}{R_a^2} + \frac{\sigma^2_{B_a}}{B_a^2}\right) + \frac{\sigma^2_{C_b} + \sigma^2_{\Phi_b}}{(\Phi_b - C_b)^2} + \frac{\sigma^2_{C_a} + \sigma^2_{\Phi_a}}{(\Phi_a - C_a)^2}\right] + \sigma^2_{B_b}\left[P_N l_{eff} + \frac{2\beta_{eff}P_N}{B_b}\right]^2 + P_N^2\left(B_b^2\sigma^2_{l_{eff}} + \sigma^2_{\beta_{eff}}\right) \quad (13)$$

where the sub-indexes a and b have the same meaning as before and it was assumed that all the parameters are uncorrelated.

The uncertainties on the parameters in Eqs. (12) and (13) were obtained as:

- $\sigma_{B_a}, \sigma_{B_b}, \sigma_{C_a}$ and σ_{C_b}: obtained directly from the least squares procedure for the fitting of the APSD's. They are given by the diagonal elements of the covariance matrix.
- $\sigma_{\beta_{eff}}$ and $\sigma_{l_{eff}}$: obtained from (Dos Santos et al., 2009).
- σ_{R_a} and σ_{R_b}: obtained as the standard deviation of the mean. The number of data containing the total count is the same as the number of averages of the APSD's.[1]
- σ_{Φ_a} and σ_{Φ_b}: obtained as the standard deviation of the mean value of the APSD's in the first plateau region (~2–9 Hz).

The partial contributions of the main terms for the uncertainty on $\sigma^2_{\rho_{gen}}$ (Eq. (12)) are shown in Table 2. It can be seen clearly that the main contributors are B_b, B_a, Φ_b^p and Φ_a^p. l_{eff} is important only for the subcritical states close to the criticality and becomes unimportant as the reactivity becomes increasingly negative. For reasons that will be explained shortly, another important parameter in the determination of ρ_{gen} is the relative power P_N. The main contributors for the $\sigma^2_{P_N}$ are given in Table 3. Here also, the main contributors are B_b, B_a, Φ_b^p and Φ_a^p. The sensitivities shown in Tables 2 and 3 are important for further experiments, where the reduction of uncertainties can be a major goal in order to get the measured data of benchmark quality.

The experimental results arising from the proposed method are shown in Fig. 5. This figure shows the total reactivity obtained as the sum of the partial ρ_{gen}, the subcriticality index (ζ) taken as negative, and the reactivity obtained from the classical point kinetic theory as: $\rho = B\ l_{eff} + \beta_{eff}$, where $B = (\rho - \beta_{eff})/l_{eff}$ is the measured prompt neutron decay constant. All the uncertainties reported in this figure are 1σ. Each experimental result, corresponding to a subcritical level, was obtained employing a more or less sensitive detector, and additional neutron sources as shown in Table 1.

Generically speaking, the measured quantities shown in Fig. 5 have the expected behavior resembling a classical S-shape. Furthermore, the uncertainties increase and also the resolution of the measured quantities becomes worse in the more subcritical states. A good part of these difficulties arises from Eq. (9) which contains explicitly the term $(1 - P_N)$ on its expression. This term requires that the relative power P_N be obtained with high accuracy and that its values be sufficiently different from 1. For the control bank positions close to critical, these conditions are achievable without difficulty. However, as the control banks are increasingly inserted, the detector count statistics and the resolution of the APSD become poorer and the relative power P_N becomes closer to 1.0. These difficulties were partly overcome with the utilization of more sensitive detectors. Another possibility not explored in the experiments would be to increase the reactivity between steps by increasing the length of the control bank insertion. This would make the relative power stay away from the value of 1.0, but, in this case, the conditions for the validity of the first order perturbation theory could be violated.

A striking result from the measurements is that the classical point kinetic theory does not describe the measured reactivities. Instead, the reactivities from this model as a function of the control bank position follow closely the subcriticality index (ζ) for the source configuration employed in the experiment. This finding might suggest that the reactivity inferred from the classical point kinetic theory is more related to the reactivity of the source than to the reactivity of the multiplying system itself.

6. Theoretical analysis

The theoretical analyses applied to the subcritical measurements were carried out in a stochastic approach employing MCNP5 (MCNP-5 X-5 Monte Carlo Team, 2003) together with its ENDF/B-VII.0 (Oblozinsky and Herman, 2006) nuclear data library and a deterministic approach based on the coupled NJOY/AMPX-II/TORT (Dos Santos et al., 2000) systems. The former deterministic methodology will be referred to as GPT-TORT. The geometric model and the material and geometric data applied in the theoretical analysis arose from LEU.COMP.THERM.082. The only exception is the position of the control banks BC1 and BC2, which in the present analysis are inserted into the core to vary the reactivity of the system. Both calculation approaches considered steps of 2.0 cm for the control bank insertion starting from the 93.41% withdrawn position.

The MCNP5 calculation scheme follows its standard way and a k-code run was requested for every control bank position. The reactivity between steps of control bank insertion was obtained as:

$$\rho = \frac{(k_{i+1} - k_i)}{(k_{i+1} \cdot k_i)}, \quad (14)$$

where ρ is the reactivity between steps, k is the effective multiplication factor and the subscript i and $i + 1$ refer to two consecutive

[1] The APSD's are obtained with a specific number of averages, for example, 900. The amount of total count values registered – in a record length time – is also 900 in this case. Thus, 900 values of total count are used to obtain a mean value and the standard deviation of the mean.

Table 2
Partial contributions of the main terms for $\sigma^2_{\rho_{gen}}$ determination in Eq. (12).

Control bank position (%)	B_b (%)	B_a (%)	Φ^p_b (%)	Φ^p_a (%)	l_{eff} (%)	Remainders (%)
93	–	–	–	–	–	–
90.5	28.4	5.2	11.1	9.1	42.8	3.5
88	32.9	8.7	7.0	20.3	29.0	2.1
85.5	35.3	15.1	20.2	11.4	16.9	1.1
83	36.5	17.0	9.7	22.6	13.2	0.8
80.5	34.4	17.5	30.6	9.6	7.4	0.5
78	28.0	18.6	22.1	29.2	1.8	0.3
75.5	34.2	24.0	11.7	25.8	4.0	0.3
70.5	41.4	19.2	10.6	20.2	8.3	0.3
65.5	43.5	18.2	25.1	8.1	4.9	0.2
63	23.8	24.2	27.4	23.2	1.3	0.1
60.5	31.4	19.4	19.1	28.9	1.0	0.1
58	36.9	26.4	13.9	20.0	2.5	0.1
55.5	37.1	32.0	13.7	16.7	0.3	0.2
53	30.4	24.7	34.4	10.2	0.2	0.2
50.5	29.2	25.5	12.9	31.8	0.5	0.2
45.5	26.6	18.7	39.8	10.0	4.8	0.2
43	25.4	20.0	13.3	39.2	1.9	0.2
40.5	29.0	28.5	23.3	17.7	1.2	0.2
35.5	30.2	23.6	21.6	21.5	2.8	0.2
33	38.1	23.3	17.7	20.3	0.2	0.3
30.5	26.9	33.0	22.3	16.3	1.2	0.3
25.5	32.9	24.6	18.3	23.4	0.4	0.3
20.5	32.6	26.6	24.0	16.0	0.5	0.4
15.5	32.9	29.0	14.2	23.3	0.2	0.4
10.5	32.0	29.7	24.3	13.5	0.0	0.5
5.5	32.7	28.9	14.9	22.6	0.5	0.5
0	34.5	34.4	13.0	17.4	0.1	0.6

Table 3
Partial contributions of the main terms for $\sigma^2_{P_N}$ determination.

Control bank position (%)	B_b (%)	B_a (%)	Φ^p_b (%)	Φ^p_a (%)	Remainders (%)
93	–	–	–	–	–
90.5	15.8	17.3	36.6	30.2	0.1
88	20.5	19.2	15.4	44.6	0.2
85.5	24.5	24.4	32.5	18.3	0.2
83	26.3	25.3	14.5	33.7	0.3
80.5	25.1	22.6	39.6	12.5	0.2
78	22.7	20.5	24.4	32.3	0.2
75.5	26.9	28.4	13.9	30.5	0.3
70.5	32.4	26.0	14.3	27.2	0.1
65.5	34.1	23.3	32.1	10.3	0.1
63	19.8	25.9	29.4	24.9	0.1
60.5	27.2	20.9	20.6	31.2	0.1
58	30.6	30.3	16.0	23.0	0.1
55.5	34.6	33.4	14.3	17.5	0.2
53	28.4	25.4	35.5	10.5	0.2
50.5	26.1	26.8	13.5	33.4	0.2
45.5	22.9	21.0	44.7	11.2	0.2
43	22.7	21.3	14.1	41.7	0.2
40.5	26.9	29.9	24.5	18.6	0.3
35.5	27.1	25.7	23.5	23.4	0.3
33	36.8	23.9	18.2	20.8	0.3
30.5	24.6	34.6	23.4	17.1	0.3
25.5	31.4	25.3	18.8	24.1	0.3
20.5	30.8	27.5	24.8	16.5	0.4
15.5	31.7	29.6	14.5	23.8	0.4
10.5	31.4	30.0	24.5	13.7	0.5
5.5	30.6	30.0	15.5	23.4	0.5
0	35.3	34.1	12.9	17.2	0.5

steps. The total reactivity is the sum of the partial reactivity between steps.

Fig. 6 shows the calculation way path for the deterministic approach. Basically, starting from ENDF/B-VII.0 nuclear data library, the well known NJOY (MacFarlane et al., 1994) system was employed to access and to process this nuclear data file in a fine group structure. The thermal neutron scattering files $S(\alpha,\beta)$, needed for

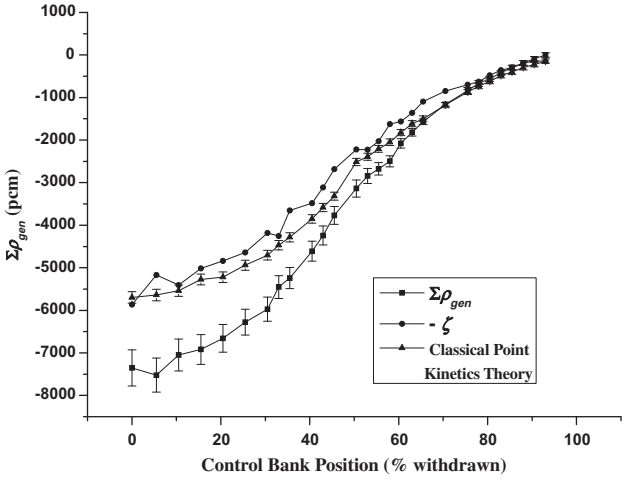

Fig. 5. Experimental results for the subcritical total reactivity ($\Sigma\rho_{gen}$), negative ζ, and the subcritical reactivity from the classical point kinetics.

hydrogen bound in water, were obtained with LEAPR module of NJOY. The RECONR, BROADR, UNRESR, THERMR and GROUPR modules of NJOY were used in order to reconstruct and to Doppler broaden the cross sections, to calculate the self-shielding effects in the unresolved resonance region, to build the scattering matrices in the thermal region, and to transform these data into multigroup parameters, respectively. The RECONR and BROADR modules of NJOY were run with 0.5% and 0.2% interpolation tolerance respectively for all nuclides. The next step was the production of set of broad group energy library using the AMPX-II (Greene, 1976) package. The pointwise and fine multigroup cross sections, which were produced in the previous steps, are transferred to AMPX-II by two in house interface modules AMPXR and BRDROL. The self-shielding treatment of the actinide resolved resonances in the neutron energy region from 0.625 eV to 5.53 keV was carried

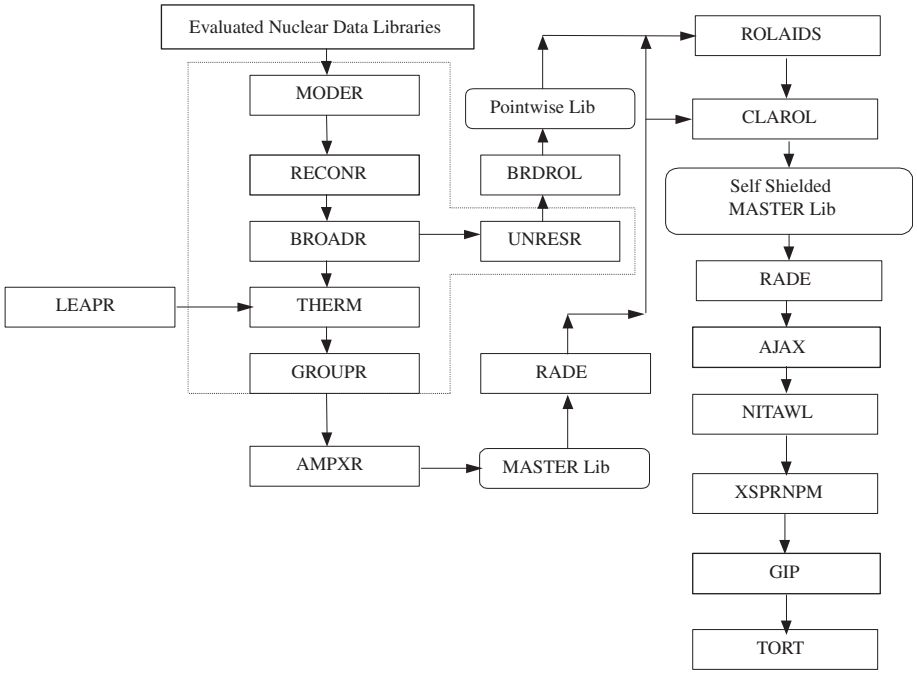

Fig. 6. Schematic diagram for the deterministic calculation methodology.

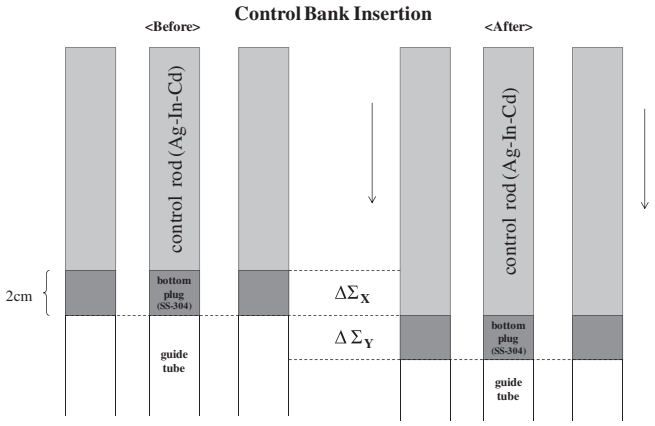

Fig. 7. Schematic diagram for cross section variations.

out using the ROLAIDS module, and the neutron spectra in the several regions of the IPEN/MB-01 reactor using XSDRNPM. Firstly, an infinite array of fuel pin cells is considered. The K_{inf} spectral calculations were performed by XSDRNPM in the fine group structure considering a white boundary condition at the outer boundary of the cylindrized unit cell. The cross sections were homogenized in a fine group level. Next, these data were merged with those of the other regions such as radial, top and bottom reflectors and so on. Finally, XSDRNPM considered radial and axial slices of the IPEN/MB-01 reactor to get the final spectra for the broad group collapsing for all regions considered in the three dimensional geometric configuration treated by TORT (3D Discrete Ordinates Code) (Rhoades and Simpson, 1991). The broad group cross sections of the control rods, guided tube, and bottom plugs of the control rods were obtained using a super-cell model. At this point, the cross section library is problem dependent. A fine multigroup structure of 620 groups (SAND-II structure) was considered to generate the broad group library, which in turn was collapsed to 16 broad groups with five upscattering as in (Dos Santos et al., 2005). The order of scattering (Legendre order expansion) was P_3 throughout the analyses. Finally, the broad group library was conveniently formatted to the TORT format using the GIP (Rhoades, 1975) program. Subsequently, using the 16 group cross sections libraries generated before, TORT performed fixed source calculations for the direct and adjoint fluxes considering a fully tri-dimensional geometric modeling of the IPEN/MB-01 reactor core. The direct flux calculations considered the Am-Be point sources shown in Fig. 4 (one at the east face of the reactor core and the other one as the start-up source of the facility) while the source for the adjoint flux calculations was taken $\gamma\sum_f/W_0$; where γ is the energy released by fission, $\sum_f$ is the macroscopic fission cross section and W_0 is the reactor power for the step under consideration.

The TORT calculations were made in steps starting from the 93.41% withdrawn position. For a given control bank position, TORT calculates the direct and adjoint neutron angular fluxes. The fully three dimensional geometric setup for the TORT calculations was considered in the X–Y–Z geometry, P_3 approximation, angular quadrature S_{16}, and 16 groups with five thermal upscattering. The mesh distribution comprised: 52 intervals in X direction, 50 in Y direction and 81 in Z direction; for a total of 210,600 intervals. These intervals were represented by 10 numbers of material zones. The boundary conditions considered were void at top and bottom and the same at the left and right borders of the problem. The convergence criterion for the source-driven calculations was set to 5.000E−04.

The quantities calculated employing the direct and the adjoint fluxes from TORT are given in Eqs. (15)–(19). The several integrals in these expressions are performed in a numerical way. In particular, the integral in the energy domain is transformed into a summation over all neutron groups. $\Delta\Sigma_t(r,E)$ and $\Delta\Sigma_s f(r,E',\Omega'\rightarrow E,\Omega)$ are the cross sections variations between steps.

$$\rho_{gen}=\frac{1}{F}\left\{-\iiint \Delta\Sigma_t(r,E)\psi(r,\Omega,E)\psi^*(r,\Omega,E)drd\Omega dE+\int\ldots\int \Delta\Sigma_s f(r,E',\Omega'\rightarrow E,\Omega)\Psi(r,\Omega',E')\Psi^*(r,\Omega,E)drd\Omega' dE' d\Omega dE\right\} \quad (15)$$

Table 4
Reactivities and effective delayed neutron parameters from the GPT-TORT approach.

Control bank position (% withdrawn)	ρ_{gen} (pcm)	ζ (pcm)	l_{eff} (μs)	β_{eff} (pcm)
93.41	0	16.8	30.58	757.37
89.74	−59.1	89.1	30.64	757.48
86.08	−109.3	170.1	30.74	757.58
82.42	−140.7	223.4	30.88	757.71
78.75	−172.9	394.1	31.04	757.82
75.09	−206.3	533.2	31.23	757.97
71.43	−239.8	692.1	31.45	758.12
67.77	−274.8	885.5	31.71	758.25
64.10	−312.1	1105.2	31.99	758.39
60.44	−346.2	1336.6	32.32	758.49
56.70	−345.8	1622.2	32.67	758.57
53.11	−535.3	1913.9	33.06	758.59
49.45	−427.2	2225.8	33.48	758.57
45.79	−504.8	2562.6	33.94	758.50
42.12	−529.0	2946.2	34.41	758.38
38.46	−540.9	3320.5	34.90	758.24
34.80	−538.1	3744.6	35.39	758.10
31.14	−520.7	4132.6	35.86	757.96
27.47	−489.7	4547.1	36.30	757.84
23.81	−447.3	4935.2	36.70	757.77
20.15	−396.3	5298.0	37.04	757.72
16.48	−340.1	5547.5	37.33	757.71
12.82	−281.9	5836.4	37.54	757.73
9.16	−224.4	6007.7	37.68	757.80
5.49	−170.8	6150.6	37.77	757.89
1.83	−126.9	6246.7	37.81	758.00

Table 5
Comparison of reactivities from the GPT-TORT to those of MCNP5.

Control Bank Position (% withdrawn)	ρ_{gen} (pcm) GPT-TORT	MCNP5 ρ (pcm)	$\Sigma\rho_{gen}$ (pcm) GPT-TORT	MCNP5 $\Sigma\rho$ (pcm)
93.41	0	0	0	0
89.74	−59.1	−125 ± 23	−59.1	−125 ± 23
86.08	−109.3	−134 ± 23	−182.0	−259 ± 23
82.42	−140.7	−92 ± 23	−327.4	−351 ± 23
78.75	−172.9	−278 ± 23	−501.3	−628 ± 23
75.09	−206.3	−217 ± 23	−704.9	−846 ± 23
71.43	−239.8	−252 ± 23	−938.2	−1098 ± 23
67.77	−274.8	−299 ± 23	−1202.9	−1396 ± 23
64.10	−312.1	−338 ± 23	−1501.1	−1734 ± 23
60.44	−346.2	−344 ± 23	−1829.0	−2078 ± 23
56.70	−345.8	−427 ± 23	−2156.1	−2505 ± 23
53.11	−535.3	−413 ± 23	−2655.1	−2918 ± 23
49.45	−427.2	−457 ± 23	−3047.2	−3375 ± 23
45.79	−504.8	−453 ± 24	−3508.3	−3828 ± 23
42.12	−529.0	−506 ± 24	−3986.0	−4335 ± 23
38.46	−540.9	−462 ± 24	−4469.4	−4796 ± 23
34.80	−538.1	−511 ± 24	−4945.8	−5308 ± 23
31.14	−520.7	−441 ± 24	−5402.8	−5749 ± 23
27.47	−489.7	−448 ± 24	−5829.5	−6198 ± 23
23.81	−447.3	−411 ± 24	−6216.8	−6609 ± 23
20.15	−396.3	−363 ± 24	−6558.2	−6972 ± 23
16.48	−340.1	−192 ± 24	−6850.0	−7164 ± 23
12.82	−281.9	−267 ± 24	−7091.4	−7431 ± 23
9.16	−224.4	−123 ± 24	−7283.6	−7553 ± 24
5.49	−170.8	−96 ± 24	−7430.9	−7650 ± 24
1.83	−126.9	−71 ± 24	−7542.8	−7720 ± 24

$$\zeta = \frac{1}{F} \tag{16}$$

$$l_{eff} = \frac{1}{F} \iiint \frac{1}{v(E)} \Psi(r,\Omega,E)\Psi^*(r,\Omega,E)dr\,d\Omega\,dE \tag{17}$$

$$\beta_{eff_j} = \frac{1}{F} \times \int \cdots \int \chi_{d_j}(E)\beta_j \nu\Sigma_f(r,E')\Psi(r,\Omega',E)\Psi^*(r,\Omega,E)dr\,d\Omega'\,dE'\,d\Omega\,dE \tag{18}$$

$$\beta_{eff} = \sum_j \beta_{eff_j} \tag{19}$$

where F is the $\int \ldots \int \chi(E)\nu\Sigma_f(r,E')\Psi(r,\Omega',E')\Psi^*(r,\Omega,E)drd\Omega'dE'd\Omega dE$; r the space coordinates; Ω the angular coordinate; E the neutron energy; $1/v$ the inverse of the neutron velocity; $\psi(r,\Omega,E)$ the direct angular neutron flux at position r, direction Ω, and energy E; $\psi^*(r,\Omega,E)$ the adjoint angular neutron flux at position r, direction Ω, and energy E; χ the fission spectra equals to: $(1-\beta)\cdot\chi_p + \beta\chi_d$; β the delayed neutron fraction equals to $\sum_j \beta_j$; $\beta_{eff,j}$ the delayed neutron fraction for delayed precursor family j; χ_p the prompt fission spectra; χ_d the delayed fission spectra; v the average number of

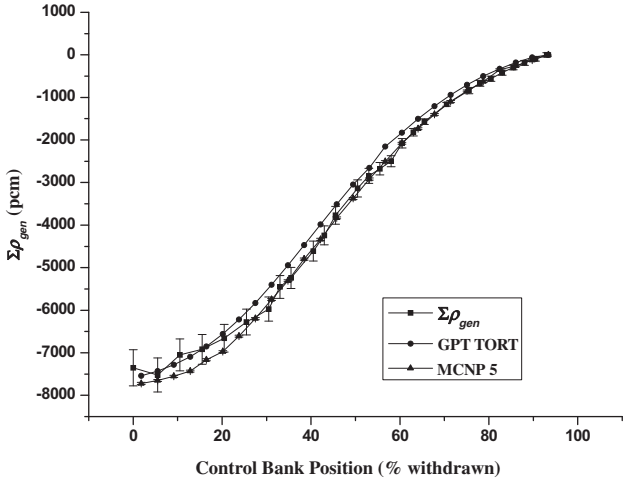

Fig. 8. Comparison of the total reactivity GPT-TORT to the experimental data.

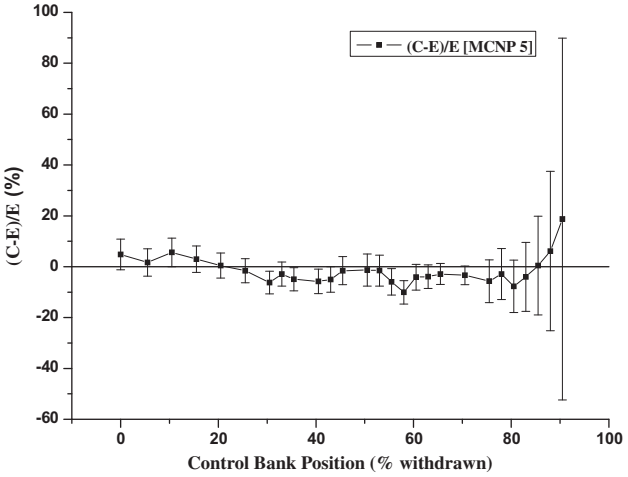

Fig. 11. Relative difference between calculated (C) and experimental (E) values for the total reactivity.

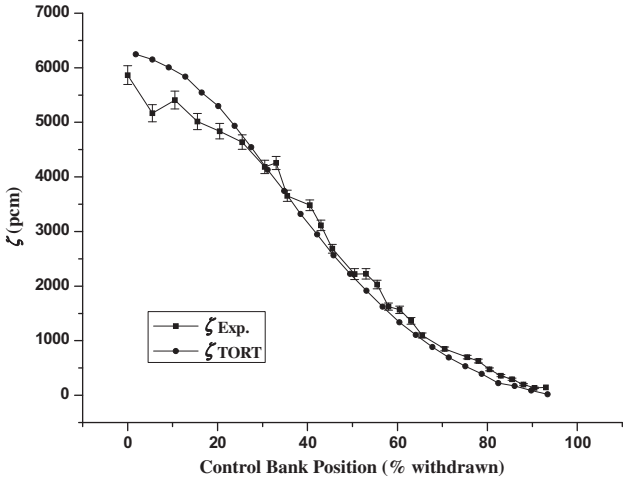

Fig. 9. Comparison of the calculated subcriticality index (ζ) to the experimental data.

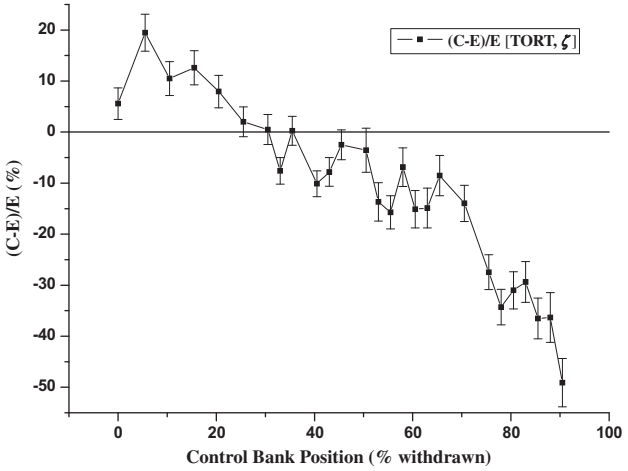

Fig. 12. Relative difference between calculated (C) and experimental (E) values for the subcriticality index (ζ).

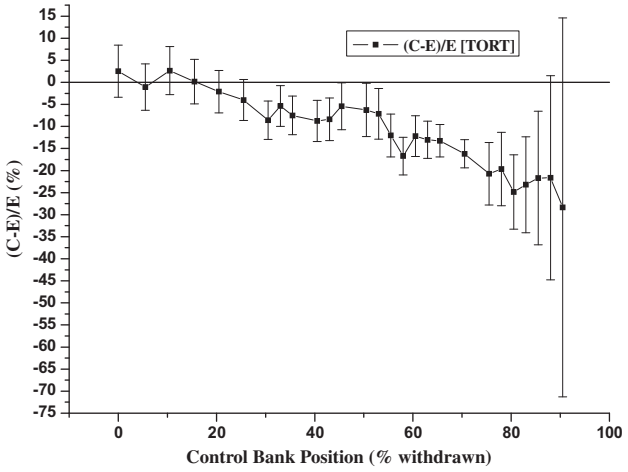

Fig. 10. Relative difference between calculated (C) and experimental (E) values for the total generalized reactivity ($\Sigma\rho_{gen}$).

neutrons produced per fission; and Σf is the macroscopic fission cross section.

The cross section variations are illustrated in Fig. 7. There are two kinds of such variations. First, as the control banks move to start a new step, the materials of the region previously occupied by the bottom plug of the control rod are replaced by those of the control rod (i.e., the region of the control rod that contains the absorber Ag–In–Cd). This is represented by $\Delta\Sigma_X$ in Fig. 7. Second, the water inside of the guide tube is now replaced by the materials of the bottom plug. This is represented by $\Delta\Sigma_Y$ in Fig. 7. Therefore, the cross section variations are the difference between the cross sections of the cell containing the control rod and those of the cell filled with the bottom plug; and the same between the latter and those of the cell of the guide tube. These are the only cross section variations for the GPT calculations.

7. The theoretical results

The results from the theoretical approach based on the coupled NJOY/AMPX-II/TORT systems are shown in Tables 4 and 5. Table 4 shows the generalized perturbation reactivity (ρ_{gen}), the subcritical index (ζ), the prompt neutron generation time (l_{eff}), and the effective delayed neutron fraction (β_{eff}); all of them as a function of the control bank position given in units of % withdrawn. $\Sigma\rho_{gen}$ given in the third column of Table 5 is the sum, up to the control bank

position under consideration, of each partial ρ_{gen}, minus the reactivity inserted by the bottom plug of the control rod in the previous steps. The reason of this subtraction is the fact that the reactivity inserted by the bottom plugs is not cumulative.

Table 5 shows the comparison of ρ_{gen} and $\Sigma\rho_{gen}$ with the reactivities obtained from MCNP5. The intention was to compare the results obtained assuming first order approximation (GPT) to those of MCNP5 based on the k_{eff} calculations (Eq. (12)).

As shown in Table 4, β_{eff} is nearly constant and l_{eff} shows some variation as a function of control bank position. There is no experimental support to attest if this behavior is credible or not. The β_{eff} behavior supports the hypothesis that this variable is constant in the experimental approach. Table 5 shows that the agreement between the reactivity inserted in steps from the GPT-TORT and those from MCNP5 as functions of the control bank positions is fairly good. This agreement is improved when the total reactivity is considered.

8. Theory/experiment comparison

Figs. 8 and 9 show respectively the comparisons of the theoretical and experimental data for $\Sigma\rho_{gen}$ and ζ. The theoretical data considered the results of the total reactivity from the GPT-TORT and MCNP5 approaches. The agreement between theoretical and experimental data is fairly good for the values of the total reactivity ($\Sigma\rho_{gen}$) from GPT-TORT and very good for the reactivities from MCNP5. The agreement in the majority of cases for the MCNP5 calculations is within the error bars of the experiment. This reinforces the ability of the proposed experimental method to measure the subcritical reactivity of multiplying systems.

The theory/experiment comparison for the subcriticality index (ζ) shown in Fig. 9 reveals some discrepancies in this calculated quantity. In this case, some more work will be needed to model the Am-Be source in the reflector. The subcritical index is strongly dependent on the source position and its geometric and material characteristics. In the TORT model, the Am-Be source was confined inside of a single mesh, which is much smaller than its real size. Also, the source materials were not modeled properly and they were simply replaced by water.

Figs. 10–12 show the relative deviation of the calculated values expressed as $(C–E)/E$, where C and E represent respectively calculated and experimental data. Here, some other details of the comparison theory/experiment become clearer. It can be seen and also quantified that the total reactivities from MCNP5 agree better to the experimental values than those of GPT-TORT. Also, as already stated, it can be seen that the agreement in the majority of cases for the MCNP5 calculations is within the error bars of the experiment. The largest discrepancies and the largest errors occur when the control banks are close to the totally withdrawn position, because in this region the total reactivity is small while its experimental uncertainty is large. The discrepancy decreases as the control banks are inserted.

The relative deviation between calculated and experimental values for the subcriticality index (ζ) in Fig. 12 shows discrepancies that are beyond of the error bars even considering the range of 3σ of the experimental values. Also, Fig. 12 shows that this quantity has a tendency to be underpredicted for the control bank position close to the totally withdrawn one, and overpredicted in the opposite sense.

9. Conclusions

The proposed experimental method for the determination of the subcritical reactivity has been demonstrated to be feasible and appropriate to deal with subcritical systems. The experiments performed for the several subcritical configurations of the IPEN/MB-01were successfully performed and they produced data of good quality. There was no omission of data and all the uncertainties have been appropriately treated. The proposed approach is based solely on measured quantities such as counting rates and the parameters arising from the least squares fitting of the APSD. Detector efficiencies, a difficult quantity to be obtained either experimentally or by a calculation approach, are not needed in this method. This experimental approach can be considered very useful for determination and description of subcritical levels in reactor systems, and it has provided very good and encouraging results. The subcritical kinetic model developed by Gandini and Salvatores has been proven to describe the physics involved in subcritical multiplying systems. The results of the experiments show clearly that the classical point kinetic theory is not able to describe the measured reactivity. The theory/experiment comparisons reveal that the agreement between the MCNP5 total reactivities and the experimental values is very good. The GPT-TORT also produced good results. Since both methodologies employ ENDF/B-VII.0 as the basic source of nuclear data, this library has performed very well in the theory/experiment comparison. In addition to that, it has been shown that the subcriticality index (ζ) from the GPT-TORT presents some discrepancies and its calculated values have a tendency to be underpredicted close to the critical state, and overpredicted for the more subcritical states. The modeling of the source together with its internal structure may be important to improve the theory/experiment comparison of the subcriticality index (ζ).

Acknowledgments

The authors are grateful to Fundação de Amparo à Pesquisa do Estado de São Paulo (FAPESP) for providing the financial supports of a doctor scholarship for Seung Min Lee under the research Project No. 2009/54838 and for the research Project 2011/50516-8.

The authors would also like to thank the operational staff of the IPEN/MB-01 reactor for their patience and efficient operation during the course of the experiment.

References

Bell, G.I., Glasstone, S., 1979. Nuclear Reactor Theory. Van Nostrand Reinhold, New York.

Bendat, J.S., Piersol, A.G., 2000. Random Data: Analysis and Measurement Procedures. John Wiley & Sons, Third Edition.

Briggs, J.B. (Ed.), 2012. International Handbook of Evaluated Criticality Safety Benchmark Experiments NEA/NSC/DOC(95)03/I. Nuclear Energy Agency, Paris (September 2012 Edition).

Cohn, C.E., 1960. A simplified theory of pile noise. Journal of Nuclear Science and Engineering 7, 472–475.

Dos Santos, A., Abe, A.Y., Mendonça, A.G., Fanaro, L.C.C.B., Andrade e Silva, G.S., 2000. Criticality Analyses Based on the Coupled NJOY/AMPX-II/TORT Systems. PHYSOR-2000, Pittsburgh, Pennsylvania.

Dos Santos, A. et al., 2004. LEU-COMP-THERM-077: critical loading configurations of the IPEN/MB-01 reactor. In: Briggs, J. Blair (Ed.), International Handbook of Evaluated Criticality Safety Benchmark Experiments. NEA/NSC/DOC (95)03/I, Paris.

Dos Santos, A. et al., 2005. The inversion point of the isothermal reactivity coefficient of the IPEN/MB-01 reactor—II: theoretical analysis. Nuclear Science and Engineering 151, 237–250.

Dos Santos, A. et al., 2006. LEU-COMP-THERM-082: critical loading configurations of the IPEN/MB-01 considering low enriched fuel and burnable poison rods. In: International Handbook of Evaluated Criticality Safety Benchmark Experiments. NEA/NSC/DOC (95)03/I, Paris.

Dos Santos, A. et al., 2008. LEU-COMP-THERM-043: critical loading configurations of the IPEN/MB-01 reactor with a heavy SS-304 reflector. In: International Handbook of Evaluated Criticality Safety Benchmark Experiments. NEA/NSC/DOC (95)03/I, Paris.

Dos Santos, A. et al., 2009. IPEN (MB01)-LWR-COEF-KIN-RESR-001: reactor physics experiments in the IPEN/MB-01 research reactor facility. In: International Handbook of Evaluated Reactor Physics Benchmark Experiments. NEA/NSC, Paris, pp. 1–142.

Dulla, S. et al., 2006. Kinetic Parameters for Source Driven Systems. PHYSOR-2006. ANS Topical Meeting on Reactor Physics Organized and Hosted by the Canadian Nuclear Society. Vancouver, BC, Canada.

Gandini, A., 2001. HGPT based sensitivity time-dependent method for the analysis of subcritical systems. Annals of Nuclear Energy 28, 1193–1217.
Gandini, A., Salvatores, M., 2002. The physics of subcritical multiplying systems. Journal of Nuclear Science and Technology 39 (6), 673–686.
Gandini, A., 2004. ADS subcriticality evaluation based on the generalized reactivity concept. Annals of Nuclear Energy 31, 813–821.
Greene, N.M. et al., 1976. AMPX-II A Modular Code System for Generation Coupled Multigroup Neutron-Gamma Libraries from ENDF/B. ORNL-TM-3706.
Hetrick, D.L., 1971. Dynamics of Nuclear Reactors. The University of Chicago Press.
Hoogenboom, J.E., Van Der Sluijs, A.R., 1988. Neutron source strength determination for on-line reactivity measurements. Annals of Nuclear Energy 15 (12), 553–559.
Kitamura, Y., Matoba, M., Misawa, T., Unesaki, H., Shiroya, S., 1999. Reactor noise experiments by using acquisition system for time series data of pulse train. Journal of Nuclear Science and Engineering 36 (8), 653–660.
MacFarlane, R.E., Muir, D.W., Bouicort, R.M., 1994. NJOY – Code System for Producing Pointwise and Multigroup Neutron and Photon Cross Sections from ENDF Data. Report LA-12740-M.
MCNP-5 X-5 Monte Carlo Team, 2003. MCNP – A General Monte Carlo N-Particle Transport Code, Version 5, LA-UR-03-1987.
Oblozinsky, O., Herman, M., 2006. Special Issue on Evaluated Nuclear Data File ENDF/B-VII.0. Nuclear Data Sheets, 107, No. 12.
Rhoades, W.A., Simpson, D.B., 1991. The TORT Three-Dimensional Discrete Ordinates Neutron/Photon Transport Code. ORNL/TM-13221.
Rhoades, W.A., 1975. The GIP Program for Preparation of Group-Organized Cross Section Libraries. PSR-75, ORNL.
Rubbia, C. et al., 2004. The TRADE Experiment: Status of the Project and Physics of the Spallation Target. PHYSOR-2004. The Physics of Fuel Cycles and Advanced Nuclear Systems: Global Developments, Chicago, Illinois, April. On CDROM, American Nuclear Society, Lagrange Park, IL.
Salvatores, M. et al., 1996. MUSE-1: A first experiment at MASURCA to validate the physics of subcritical multiplying systems relevant to ADS. In: 2nd ADTT Conf. Kalmar, Sweden.
Shi, Y.Q., Zhu, Q.F., Tao, H., 2005. Review and research of the neutron source multiplication method in nuclear critical safety. Nuclear Technology 149 (1), 122–127.
Shimazu, Y., Naing, W., 2005. Some technical issues on continuous subcriticality monitoring by a digital reactivity meter during criticality approach. Journal of Nuclear Science and Engineering 42 (6), 515–524.
Suzuki, E., 1966. A method for measuring absolute reactor power through neutron fluctuation. Journal of Nuclear Science and Engineering 3 (3), 98–105.